Carbohydrate Polymers 86 (2011) 877–882

Contents lists available at ScienceDirect

Carbohydrate Polymers

journal homepage: www.elsevier.com/locate/carbpol

# Preparation and properties of layered double hydroxide–carboxymethylcellulose sodium/glycerol plasticized starch nanocomposites

Dongliang Wu [a], Peter R. Chang [b], Xiaofei Ma [a,*]

[a] Chemistry Department, School of Science, Tianjin University, Tianjin 300072, China
[b] Bioproducts and Bioprocesses National Science Program, Agriculture and Agri-Food Canada, 107 Science Place, Saskatoon, SK S7N 0X2, Canada

ARTICLE INFO

*Article history:*
Received 4 May 2011
Received in revised form 17 May 2011
Accepted 18 May 2011
Available online 26 May 2011

*Keywords:*
Layered double hydroxide (LDH)
Carboxymethylcellulose sodium (CMC)
Starch
Nanocomposites

ABSTRACT

The Zn–Al layered double hydroxide (LDH) was fabricated using carboxymethyl-cellulose sodium (CMC) as the stabilizer in aqueous solution, and then used as the filler to prepare LDH–CMC/glycerol plasticized-starch (GPS) nanocomposites in the casting process. Transmission electron microscopy exhibited the platelets of LDH–CMC with a lateral size of 30–60 nm and the thickness of 5–10 nm. X-ray diffraction showed that the presence of CMC decreased the thickness of LDH. The chemical formulas of LDH was $[Zn_{0.64}{\cdot}Al_{0.36}{\cdot}(OH)_2]Cl_{0.36}{\cdot}nH_2O$, and the content of CMC was about 37.5 wt%. LDH–CMC possessed the good stability in water because of hydrophilic CMC components and the smaller size of each LDH stack. A low loading of LDH–CMC (below 6 wt%) could obviously improve mechanical properties and water vapor barrier of the nanocomposites, because LDH–CMC could form the good interaction with GPS matrix.



## 1. Introduction

The starch-based biodegradable materials have gained worldwide attention because of their biodegradability, renewability and low cost. Plasticized starch (PS)/layered inorganic nanocomposites can improve barrier properties, reduce flammability and improve mechanical properties of pure PS. There have been many reports on various kinds of starch-based layered inorganic nanocomposites, such as montmorillonite (MMT), hectorite, Kaolinite and layered double hydroxides (LDHs). Park et al. (2002) used three organically modified MMTs with different ammonium cations and one unmodified MMT to prepare PS/MMT composites by melt processing. Huang, Yu, Ma, & Jin (2005) prepared ethanolamine-activated MMT (EMMT). Using a similar method, citric acid-activated MMT (CMMT) is also obtained (Huang, Yu, & Ma, 2006). A method (Ma, Yu, & Wang, 2007) is developed to prepare PS/MMT–sorbitol nanocomposites without the addition of organic solution or generating waste water. In the approach, MMT layers are intercalated by sorbitol, and a MMT–sorbitol complex is thus obtained in the first melt extrusion. During the second melt extrusion, both sorbitol in the MMT–sorbitol complex and formamide act as plasticizers to plasticize starch, and the resultant PS is intercalated into the MMT layers. Chiou et al. (2007) use a twin-screw extruder to extrude wheat starch/MMT nanocomposites containing different levels of glycerol and water. Tang, Alavi, & Herald (2008) conclude that the degree of MMT exfoliation in PS/MMT nanocomposites increase with the decreasing of glycerol contents. Compared to glycerol as plasticizer of starch, urea and formamide can improve the degree of MMT exfoliation. Natural hectorite or modified hectorite is also used to prepare the composites with PS by melt-processing on a twin roll mill (Chen and Evans, 2005). Kaolinite interacts with small polar molecules, such as dimethyl sulfoxide (DMSO), which are used as precursors for the intercalation of starch. Kaolinite/DMSO/carboxymethyl starch nanocomposites are prepared by Wang and Zhao (2006).

LDHs have received considerable attention because of their applications as catalysts, ion exchangers, absorbents, ceramic precursors, drug carriers and polymer stabilizers. LDHs can be described by the ideal formula $[M^{II}{}_{1-x}M^{III}{}_x(OH)_2]_{intra}[A^{m-}{}_{x/m}{\cdot}nH_2O]_{inter}$, where '$M^{II}$' and '$M^{III}$' are metal cations, 'A' is the anion, and 'intra' and 'inter' denote the intralayer domain and the interlayer space, respectively. The structure consists of brucitelike layers constituted of edge-sharing $M(OH)_6$ octahedra. Partial '$M^{II}$' and '$M^{III}$' substitution induces a positive charge for the layers, balanced with the presence of the interlayered anions (Leroux and Besse, 2001). The starch–LDH nanocomposites are prepared by growing LDH crystallites in starch (or acid-modified starch) dispersions under hydrothermal treatment conditions (Chung and Lai, 2010). During the processing, the LDH nuclei are first precipitated in the partially gelatinized starch dispersion, and then gradually age in the dispersed starch under hydrothermal conditions. In this way, LDH can be embedded in a starch matrix.

Since carboxymethylcellulose (CMC) can form the interaction with metal ions, CMC has been used as a stabilizing agent of metal

* Corresponding author. Tel.: +86 22 27406144; fax: +86 22 27403475.
*E-mail address:* maxiaofei@tju.edu.cn (X. Ma).

0144-8617/$ – see front matter. 
doi:10.1016/j.carbpol.2011.05.030

oxide nanoparticles. It plays a very important role on the preparation of both metal oxide-CMC and PS/metal oxide-CMC composites (Chang, Yu, & Ma, 2009; Yu, Yang, Liu, & Ma, 2009). In this work, Zn–Al LDH is fabricated with CMC as the stabilizer in aqueous solution, and then used as the filler to prepare LDH–CMC/glycerol plasticized-starch (GPS) composites. CMC can disperse LDH well and LDH with less layer numbers is obtained in LDH–CMC. As the filler, LDH–CMC can form the strong interaction with GPS matrix because of chemical similarities.

## 2. Experimental

### 2.1. Materials

Potato starch was supplied by Manitoba Starch Products (Manitoba, Canada). Carboxymethyl cellulose sodium (CMC) was analytical grade and obtained from Tianjin Fine Chemical Institute (Tianjin, China). Glycerol, zinc nitrate hexahydrate, aluminium chloride and sodium hydroxide were of analytical grade from Tianjin Chemical Reagent Factory (Tianjin, China).

### 2.2. The Preparation of LDH–CMC

0.5 g CMC was added to 150 ml distilled water. The mixture was heated at 90 °C for about 10 min with constant stirring for the complete dissolution of CMC. The solution was cooled to the room temperature. Aluminium chloride hexahydrate, 0.6375 g and zinc chloride 1.002 g were added in the solution, and then 35 ml of sodium hydroxide solution (0.1 mol/l) was added drop-wise with constant stirring under $N_2$. The pH of the final mixtures was controlled in the range of 9–10. The mixtures were aged for 20 h and then washed 3 times with distilled water. After washing with ethanol, the LDH–CMC was dried at 30 °C for 24 h.

### 2.3. The preparation of LDH–CMC/GPS nanocomposites

LDH–CMC was dispersed into the solution of distilled water (80 ml) and glycerol (0.9 g) using ultrasonication for 10 min. 3 g potato starch was added. The filler loading level (0, 2, 4, 6 or 8 wt%) was based on the potato starch. The mixture was heated at 95 °C for 0.5 h for the plasticization of starch with constant stirring. The mixture was cast into a membrane on a dish. The formed solid-like membranes were placed in an air-circulating oven at 50 °C until they were dry (about 4–6 h). The composite films of LDH–CMC/GPS were preconditioned in a climate chamber at 25 °C and 50% RH for at least 48 h prior to the testing.

### 2.4. Characterization

#### 2.4.1. Fourier transform infrared spectroscopy (FTIR)

FTIR spectra of CMC and LDH–CMC were performed at 2 $cm^{-1}$ resolution with BIO-RAD FTS3000 IR Spectrum Scanner. Typically, 64 scans were signal-averaged to reduce spectral noise.

#### 2.4.2. Transmission electron microscopy (TEM) and energy dispersive X-ray spectroscopy (EDS)

The suspension of LDH–CMC platelets was dropped on a copper grid which was coated with a carbon film, then air-dried, and examined using Tecnai G2 F20 TEM. And the atomic ratio of Al/Zn/Cl (12/23/12.4) was recorded by EDS.

### 2.5. X-ray diffraction (XRD)

LDH–CMC was placed in a sample holder for XRD. XRD patterns were recorded in reflection mode by a D/MAX2500 diffractometer operated at a CuKα wavelength of 1.542 Å.

#### 2.5.1. Thermogravimetric (TG) analysis

Thermal properties of CMC, LDH–CMC and the nanocomposites were measured with a ZTY-ZP type thermal analyzer. The weights of samples were about 10 mg, and heated from room temperature to 600 °C at a heating rate of 15 °C/min in a nitrogen atmosphere.

#### 2.5.2. UV-visible (UV-vis) spectra

The UV-visible spectra of different concentrations LDH–CMC in water were recorded from 200 to 800 nm using a UV–vis spectrophotometer model U-1800, Hitachi Company.

#### 2.5.3. Scanning electron microscopy (SEM)

The fracture surfaces of nanocomposites were tested by a Nanosem 430 Scanning Electron Microscope. The composites were cooled in liquid nitrogen, and then broken. The fracture faces were vacuum coated with gold for SEM.

#### 2.5.4. Mechanical testing

The Testometric AX M350-10KN Materials Testing Machine was operated at a crosshead speed of 50 mm/min for tensile testing (ISO 1184–1983 standard). Samples were conditioned at 25 °C and 50% RH for 48 h before testing. The data was averaged over 6–8 specimens.

#### 2.5.5. Water vapor permeability (WVP)

WVP tests were carried out by ASTM method E96 (1996) with some modifications (Yu et al., 2009). The films were cut into circles, sealed over with melted paraffin, and stored in a desiccator at 25 °C. RH0% was maintained using anhydrous calcium chloride in the cell. Each cell was placed in a desiccator containing saturated sodium chloride to provide a constant RH75%. Water vapor transport was determined by the weight gain of the permeation cell. Changes in the weight of the cell were recorded as a function of time. Slopes were calculated by linear regression (weight change vs. time) and correlation coefficients for all reported data were >0.99. The water vapor transmission rate (WVTR) was defined as the slope (g/s) divided by the transfer area ($m^2$). After the permeation tests, film thickness was measured and WVP (g $Pa^{-1}$ $s^{-1}$ $m^{-1}$) was calculated as:

$$\mathrm{WVP} = \frac{\mathrm{WVTR}}{P(R_1 - R_2)} \cdot x$$

where $P$ is the saturation vapor pressure of water (Pa) at the test temperature (25 °C), $R_1$ is the RH in the desiccator, $R_2$, the RH in the permeation cell and $x$ is the film thickness (m). Under these conditions, the driving force $[P(R_1 - R_2)]$ is 1753.55 Pa.

## 3. Results and discussion

### 3.1. Characterization of LDH–CMC

In Fig. 1(a), the FTIR spectra of CMC exhibited the broad band centered at 3428 $cm^{-1}$, attributed to a wide distribution of hydrogen-bonded hydroxyl groups. And the peak about C–H stretching associated with the ring methane hydrogen atoms appeared at 2918 $cm^{-1}$. The peaks at 1433 and 1610 $cm^{-1}$ were related to the symmetrical and asymmetrical stretching vibrations of the carboxylate groups (Rosca, Popa, & Lisa, 2005). The absorption bands between 1000 and 1200 $cm^{-1}$ were ascribed to characteristic of the –C–O– stretching on polysaccharide skeleton. Compared to the FTIR spectra of CMC, LDH–CMC recorded the new peak at about 431 $cm^{-1}$, which was attributed to the metal–oxygen bond in the brucite-like lattice (Darder, Lopez-Blanco, Aranda, Leroux, & Ruiz-Hitzky, 2005; Wang et al., 2011), indicating that the LDH structure was truly formed when biopolymer was incorporated.

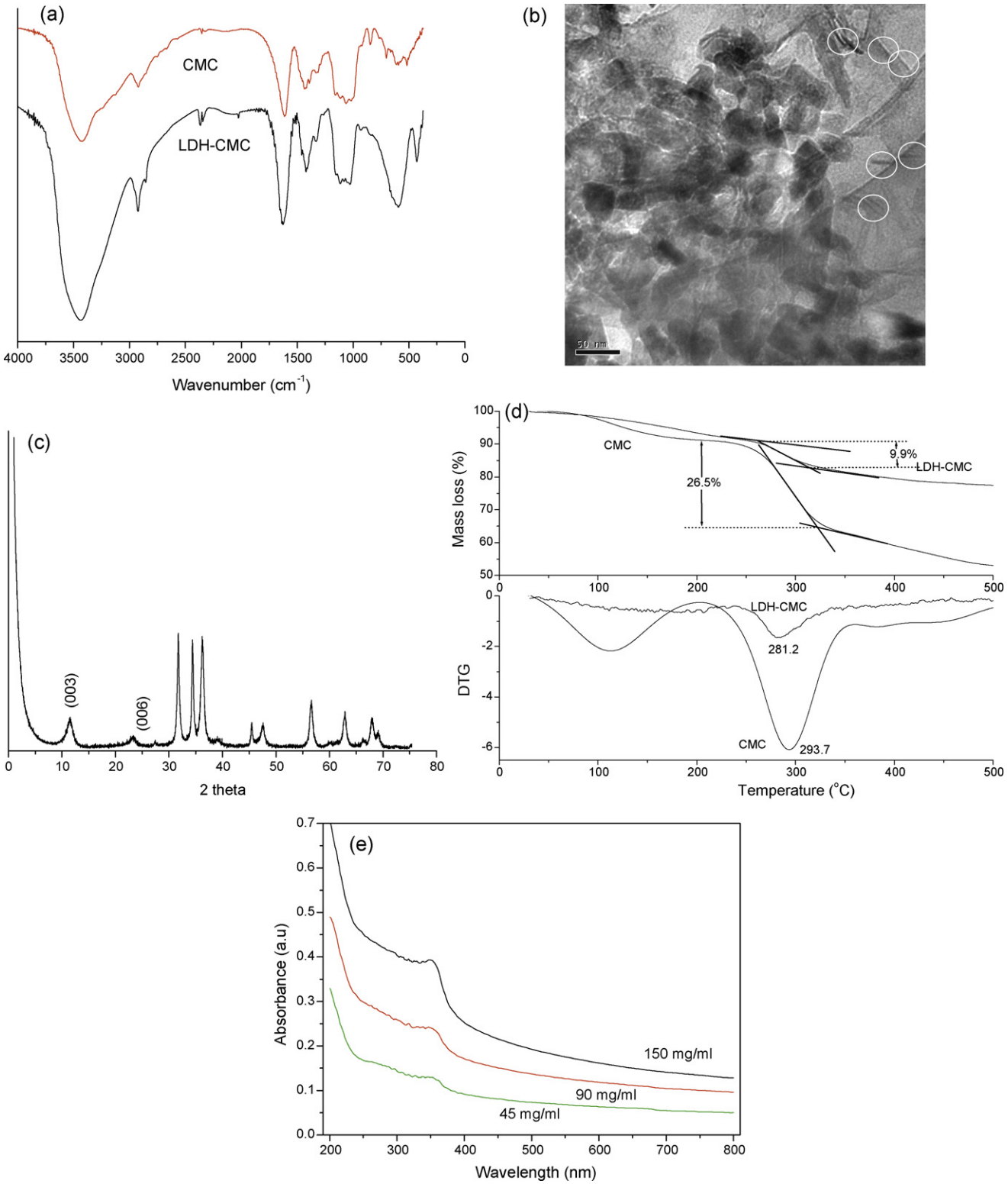


**Fig. 1.** (a) FTIR of spectra of CMC and LDH–CMC, (b) TEM of LDH–CMC, (c) XRD patterns of LDH–CMC, (d) the thermogravimetric (TG) and derivative thermogravimetric (DTG) curves of CMC and LDH–CMC and (e) UV-visible absorption spectra of LDH–CMC in water at the different concentrations.

As shown in Fig. 1(b), LDH–CMC exhibited the platelets with a lateral size of 30–60 nm and the thickness of 5–10 nm. The thickness was shown with white circles. And it was observed that the LDH platelets were encapsulated into CMC. Because polysaccharides could form complexes with metal ions due to their high number of coordinating functional groups (hydroxyl and glucoside groups) (Taubert and Wegner, 2002), it was likely that the majority of the metal ions were closely associated with the CMC molecules. Therefore nucleation and initial crystal growth of hydroxides may preferentially occur on CMC. And the atomic

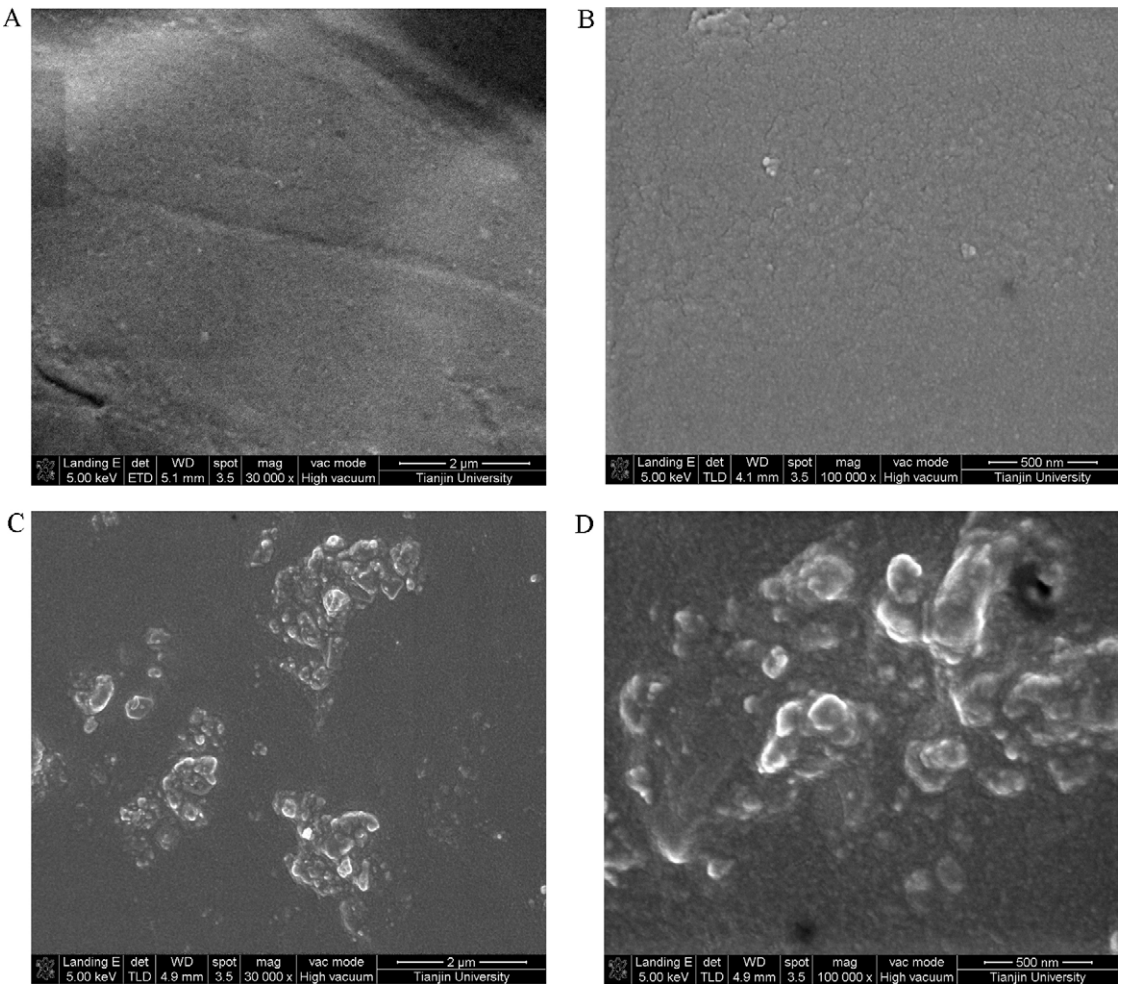


**Fig. 2.** SEM micrograph of the fragile fractured surface of the nanocomposites with different LDH–CMC contents (a and b) 2 wt% and (c and d) 8 wt%.

ratio of Al/Zn/Cl (12/23/12.4) was recorded by EDS in TEM testing. The chemical formulas of LDH in LDH–CMC was proposed to be $[Zn_{0.64}{\cdot}Al_{0.36}{\cdot}(OH)_2]Cl_{0.36}{\cdot}nH_2O$.

Fig. 1(c) revealed the XRD pattern of LDH–CMC. When LDH was prepared in the CMC, the interlayer spacing of LDH crystallites remained at 7.5–7.9 Å ($2\theta = 11.2$–$11.8^\circ$). The estimated thickness of LDH was 5.8–6.2 nm using Scherrer's equation based on the full width at half maximum (FWHM) of the (0 0 3) peak. Scherrer's formula (Shen, Bao, & Yanagisawa, 2006) is expressed with $D = 0.89\lambda/(\beta \cos\theta)$, where $\lambda$ is the wavelength (CuK$\alpha$), $\beta$ is the full width at the half-maximum of XRD peaks and $\theta$ is the diffraction angle. This crystal size was approximately 7–8 layers of brucite-like sheets, which were far below 29 layers per stack (Chung and Lai, 2010) and 17 layers (Chen, Gunawan, & Xu, 2011) of the pristine LDH. This result was similar to LDH synthesized in the starch slurry under hydrothermal treatment (Chung and Lai, 2010). The presence of CMC decreased the layer numbers, i.e. the thickness of LDH, although the interlayer spacing of LDH crystallites unchanged. Polysaccharides presented the dynamic supramolecular associations facilitated by inter- and intra-molecular hydrogen bonding, which could be related to the low layer numbers of LDHs.

The thermogravimetric (TG) and Derivative thermogravimetric (DTG) curves of CMC and LDH–CMC were shown in Fig. 1(d). The decomposed temperature was the temperature at maximum rate of mass loss, i.e. the peak temperature shown in DTG curves. The decomposed temperature of CMC was 293.7 °C, while that of CMC in LDH–CMC was 281.2 °C. CMC exhibited the better thermal stability than CMC in LDH–CMC. It could be ascribed to the degradation of CMC in the preparation of LDH. The LDH–CMC showed a weight loss of 9.9 wt% at the decomposed temperature of CMC. The quantity of CMC was calculated by matching the percentage weight loss of LDH–CMC to the percentage of weight loss of CMC at the decomposed temperature (about 26.5 wt%). The content of CMC in LDH–CMC was estimated to be about 37.3 wt%.

Fig. 1(e) showed the UV-vis spectra of different concentrations of LDH–CMC in distilled water. The absorption peak at 351 nm was attributed to the characteristic absorption of ZnO in LDH. The linear relationship between the observed absorption peak and the LDH–CMC concentrations indicated that the optical behavior that was typically caused by aggregation of any multi-molecular species was not displayed in the tested concentration range (Wu et al., 2007). LDH–CMC exhibited the good stability in water because of hydrophilic CMC components and the smaller size (layer number) of each LDH stack, which were helpful for the uniform dispersion of LDH–CMC fillers in GPS matrix.

### 3.2. The properties of LDH–CMC/GPS nanocomposites

#### 3.2.1. SEM of nanocomposites

The dispersion of LDH–CMC in the matrix was shown in Fig. 2. LDH–CMC could be evenly dispersed in GPS matrix at low loading (2 wt%). The agglomeration of LDH–CMC appeared in the LDH–CMC/GPS composites with higher LDH–CMC contents (8 wt%). In addition, the surface of LDH–CMC appeared to be covered by GPS, which was related to strong interaction between

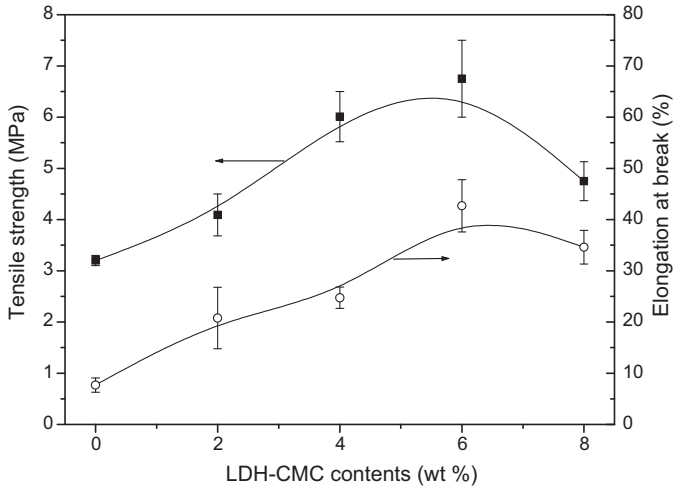


**Fig. 3.** The effect of LDH–CMC contents on tensile yield strength and elongation at break of the composites.

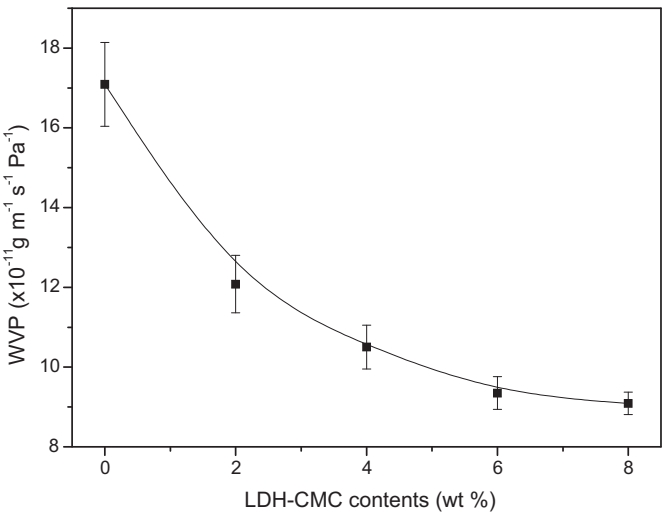


**Fig. 4.** The effect of LDH–CMC contents on water vapor permeability of the composites.

CMC in LDH–CMC filler and GPS matrix because of their similar polysaccharide structure.

### 3.2.2. Mechanical properties of nanocomposites

Fig. 3 revealed the effect of LDH–CMC contents on the mechanical properties of the nanocomposites. As the filler in the GPS matrix, LDH–CMC had an obvious reinforcing effect. With the increasing of LDH–CMC contents, the tensile strength increased. When LDH–CMC contents varied from 0 to 6 wt%, the tensile strength increased from 3.2 MPa to 6.75 MPa. The improvement of tensile strength was related to the good interfacial interaction between the GPS matrix and the LDH–CMC filler because starch and CMC possessed the similar polysaccharide structures.

However, when GPS matrix was loaded with more LDH–CMC filler (8 wt%), the tensile strength of the nanocomposites decreased to 4.75 MPa. The agglomeration of LDH–CMC, as shown in Fig. 2(c and d), actually reduced the effective filler loading. Generally, the well-dispersed fillers could constrain the surrounding polymers, decrease the mobility of matrix chains, and further result in the higher tensile strength and lower elongation at break. However, the elongation at break and tensile strength of the LDH–CMC/GPS composites exhibited the same tendency with the increasing of LDH–CMC contents. Similarly, the addition of CMC fillers could improve the tensile strength and elongation at break of GPS (Ma, Chang, & Yu, 2008).

### 3.2.3. WVP of nanocomposites

Fig. 4 exhibited the moisture transport through the nanocomposite films with different LDH–CMC contents. WVP of nanocomposites decreased with the increasing of LDH–CMC contents at RH 75%. Water vapor easily went through GPS film with the highest WVP values of $17.09 \times 10^{-11}$ g m$^{-1}$ s$^{-1}$ Pa$^{-1}$. With the increasing of LDH–CMC contents, WVP values decreased obviously. When LDH–CMC contents reached above 6 wt% (as shown in SEM), WVP values decreased a little. The addition of LDH–CMC probably introduced a tortuous path for water molecule to pass through (Chang, Jian, Yu, & Ma, 2010). At the low LDH–CMC loading contents (below 6 wt%), LDH–CMC could disperse well in the matrix. There were few paths for water molecule to pass through. At the high

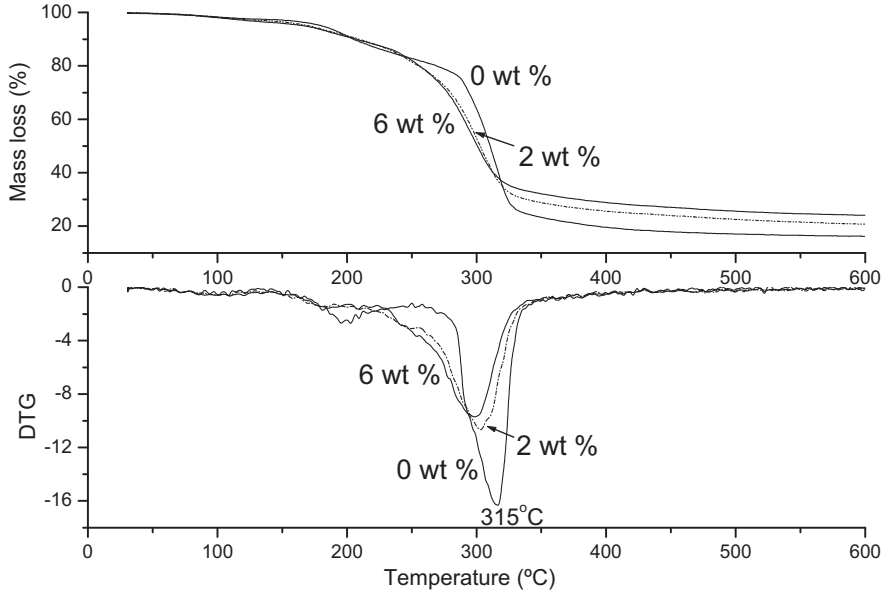


**Fig. 5.** The effect of LDH–CMC contents on the thermal stability of the composites.

contents of LDH–CMC, the aggregation of LDH–CMC could counteract the addition of LDH–CMC. Generally, the nanocomposites exhibited moisture barrier in comparison with pure GPS film.

### 3.2.4. Thermal stability of nanocomposites

TG and DTG curves of LDH–CMC/GPS nanocomposites were shown in Fig. 5. The degradation of GPS took place at 315 °C, while LDH–CMC/GPS nanocomposites containing 2 wt% and 6 wt% LDH–CMC degraded at lower 300 °C and 297 °C, respectively. The addition of LDH unexpectedly decreased the thermal stability of the nanocomposites. It was also noted that the residues at the high temperature were improved with increased loading of LDH–CMC. The reason could be that CMC had poor thermal stability. The decomposition temperature of CMC was 293.7 °C, as shown in Fig. 1(d). The decomposition of CMC components could weak the interaction between LDH filler and GPS matrix, and simultaneously accelerate the decomposition of starch. GPS/CMC composites exhibited the similar results (Ma et al., 2008).

## 4. Conclusions

By using CMC as the stabilizer, the LDH–CMC was prepared with a lateral size of 30–60 nm and the thickness of 5–10 nm. The chemical formulas of LDH was $[Zn_{0.64}{\cdot}Al_{0.36}(OH)_2]Cl_{0.36}{\cdot}nH_2O$, and the content of CMC was about 37.3 wt%. The introduction of CMC could improve the good stability in water because of hydrophilic CMC components and the smaller size (layer number) of each LDH stack, which were helpful for the uniform dispersion of LDH–CMC fillers in GPS matrix. At the low loading of LDH–CMC can obviously improve tensile strength and elongation at break, and decrease the water vapor permeability of LDH–CMC/GPS nanocomposites in comparison with pure GPS. More LDH–CMC contents (8 wt%) could result in the agglomeration of LDH–CMC in the LDH–CMC/GPS composites, which decreased the effective filler loading, and reduced mechanical properties and WVP values. In addition, the decomposition of CMC components in LDH–CMC could weak the interaction between LDH filler and GPS matrix, and facilitate the decomposition of starch matrix, so LDH–CMC decreased the thermal stability of the nanocomposites.

## References


Chang, P. R., Jian, R. J., Yu, J. G., & Ma, X. F. (2010). Fabrication and characterization of chitosan nanoparticles/plasticized-starch composites. *Food Chemistry*, *120*, 736–774.

Chang, P. R., Yu, J. G., & Ma, X. F. (2009). Fabrication and characterization of $Sb_2O_3$/carboxymethyl cellulose sodium and the properties of plasticized starch composite films. *Macromolecular Materials and Engineering*, *294*, 762–767.

Chen, B. Q., & Evans, J. R. G. (2005). Thermoplastic starch–clay nanocomposites and their characteristics. *Carbohydrate Polymers*, *61*, 455–463.

Chen, C. P., Gunawan, P., & Xu, R. (2011). Self-assembled $Fe_3O_4$-layered double hydroxide colloidal nanohybrids with excellent performance for treatment of organic dyes in water. *Journal of Materials Chemistry*, *21*, 1218–1225.

Chiou, B. S., Wood, D., Yee, E., Imam, S. H., Glenn, G. M., & Orts, W. J. (2007). Extruded starch–nanoclay nanocomposites: Effects of glycerol and nanoclay concentration. *Polymer Engineering and Science*, *47*, 1898–1904.

Chung, Y. L., & Lai, H. M. (2010). Preparation and properties of biodegradable starch-layered double hydroxide nanocomposites. *Carbohydrate Polymers*, *80*, 525–532.

Darder, M., Lopez-Blanco, M., Aranda, P., Leroux, F., & Ruiz-Hitzky, E. (2005). Bionanocomposites based on layered double hydroxides. *Chemistry of Materials*, *17*, 1969–1977.

Huang, M. F., Yu, J. G., & Ma, X. F. (2006). High mechanical performance MMT-urea and formamide-plasticized thermoplastic cornstarch biodegradable nanocomposites. *Carbohydrate Polymers*, *63*, 393–399.

Huang, M. F., Yu, J. G., Ma, X. F., & Jin, P. (2005). High performance biodegradable thermoplastic starch – EMMT nanoplastics. *Polymer*, *46*, 3157–3162.

Leroux, F., & Besse, J. P. (2001). Polymer interleaved layered double hydroxide: A new emerging class of nanocomposites. *Chemistry of Materials*, *13*, 3507–3515.

Ma, X. F., Chang, P. R., & Yu, J. G. (2008). Properties of biodegradable thermoplastic pea starch/carboxymethyl cellulose and pea starch/microcrystalline cellulose composites. *Carbohydrate Polymers*, *72*, 369–375.

Ma, X. F., Yu, J. G., & Wang, N. (2007). Production of thermoplastic starch/MMT–sorbitol nanocomposites by dual-melt extrusion processing. *Macromolecular Materials and Engineering*, *292*, 723–728.

Park, H. M., Li, X. C., Jin, C. Z., Park, C. Y., Cho, W. J., & Ha, C. S. (2002). Preparation and properties of biodegradable thermoplastic starch/clay hybrids. *Macromolecular Materials and Engineering*, *287*, 553–558.

Rosca, C., Popa, M. I., & Lisa, G. (2005). Interaction of chitosan with natural or synthetic anionic polyelectrolytes. 1. The chitosan–carboxymethylcellulose complex. *Carbohydrate Polymers*, *62*, 35–41.

Shen, L. M., Bao, N. Z., & Yanagisawa, K. (2006). Direct synthesis of ZnO nanoparticles by a solution-free mechanochemical reaction. *Nanotechnology*, *17*, 5117–5123.

Tang, X. Z., Alavi, S., & Herald, T. J. (2008). Effects of plasticizers on the structure and properties of starch–clay nanocomposites films. *Carbohydrate Polymers*, *74*, 552–558.

Taubert, A., & Wegner, G. (2002). Formation of uniform and monodisperse zincite crystals in the presence of soluble starch. *Journal of Materials Chemistry*, *12*, 805–807.

Wang, B. X., & Zhao, X. P. (2006). The influence of intercalation rate and degree of substitution on the electrorheological activity of a novel ternary intercalated nanocomposite. *Journal of Solid State Chemistry*, *179*, 949–954.

Wang, D. Y., Leuteritz, A., Kutlu, B., Landwehr, M. A., Jehnichen, D., Wagenknecht, U., et al. (2011). Preparation and investigation of the combustion behavior of polypropylene/organomodified MgAl–LDH micro-nanocomposite. *Journal of Alloys and Compounds*, *509*, 3497–3501.

Wu, Z. G., Feng, W., Feng, Y. Y., Liu, Q., Xu, X. H., & Sekino, T. (2007). Preparation and characterization of chitosan-grafted multiwalled carbon nanotubes and their electrochemical properties. *Carbon*, *45*, 1212–1218.

Yu, J. G., Yang, J. W., Liu, B. X., & Ma, X. F. (2009). Preparation and characterization of glycerol plasticized-pea starch/ZnO–carboxymethylcellulose sodium nanocomposites. *Bioresource Technology*, *100*, 2832–2841.